AIAA 81-4258

Design of Low-Drag Axisymmetric Shapes by the Inverse Method

Charles Dalton*
University of Houston, Houston, Texas
and
M.F. Zedan†
Brown & Root, Inc., Houston, Texas

The inverse method is applied to the design of a low-drag aerodynamics shape. The problem treated is an axisymmetric body generated by means of an axial distribution of line sources and sinks. Recommended low-drag shapes are examined to determine if modification of the external velocity will lead to a reduced drag by body reshaping. It is found that the delay of transition on a particular known body shape can be achieved. This results in an improved body shape with lower drag coefficient and better transition characteristics at a volume Reynolds number of 5×10^7. This study demonstrates the importance of the inverse method in determining low-drag shapes.

Nomenclature

A = reference area
C_j = vector in velocity equations
C_{DV} = volume drag coefficient
C_f = skin-friction coefficient
D = drag
FR = fineness ratio
H = shape factor
L = body length
M = number of unknown coefficients
q = velocity on surface $= \sqrt{u^2 + v^2}$
r = radial coordinate
R_θ = momentum thickness Reynolds number
R_L = length Reynolds number
R_V = volume Reynolds number
S = slope of meridian line on surface
$\bar{U}_{ij}$ = geometric matrix in u equation
U = x direction velocity
U_∞ = uniform approach velocity
v = r direction velocity
V = body volume
$\bar{V}_{ij}$ = geometric matrix in v equation
x = coordinate in direction of body length
x_n = distance from leading edge to first element
x_t = distance from trailing edge to last element end
ρ = fluid density
ν = kinematic viscosity
Ψ = stream function
σ_ξ = strength of variable intensity source
ξ = dummy variable of integration
$\bar{\Psi}_{ij}$ = geometric matrix in Ψ equation
θ = axisymmetric momentum thickness
δ^* = axisymmetric displacement thickness

Introduction

THE design of low-drag axisymmetric body shapes is currently receiving considerable attention in the engineering community. The motivation is the need to develop more efficient shapes suitable for airship, torpedos, and submarine applications. With the increasing cost of energy, recent studies[1] demonstrated the feasibility of the use of airships in long-distance handling of large bulky cargo. Most of the analyses on airship aerodynamics are quite old; thus, it is timely to reconsider the airship shape using the latest design considerations to reduce the drag. Underwater vehicles also have the potential for significant drag reduction, as has been pointed out by a number of investigators. A likely opportunity for drag reduction has to do with body shaping to produce as long a run of laminar boundary layer (LBL) along the body surface as possible.

For a body of revolution in an incompressible axial flow, the total drag may be divided into two parts. The first part is due to fluid friction (viscosity) along the body surface, while the second is due to the net pressure force acting on the body in the direction of the undisturbed flow. For a streamlined body with a thin and attached boundary layer, pressure drag is negligible compared to viscous drag. Since the effects of viscosity are confined to the boundary layer, friction drag can be reduced by controlling the growth of the boundary layer. An effective and economical method to achieve that is by appropriate body shaping. The classical approach to shape design is to start with a certain geometry that conceivably satisfies the requirements, and then to manipulate the geometrical parameters to achieve lower drag and/or enhance other required characteristics. This procedure can probably be classified as a "trial-and-error" approach; the success depends mainly on the individual designer's experience. An alternative procedure is to use the inverse-problem approach. In such an approach, a prescribed velocity distribution is input and the corresponding shape is computed. Obviously, it is easier to manipulate the velocity distribution as compared to the body geometry to achieve specific requirements. This is due simply to the fact that cavitation, flow separation, and boundary-layer transition are related to the characteristics of the velocity distribution in a more direct manner than to the body geometry. Thus, the inverse-problem approach, while not eliminating trial and error, reduces it substantially; it is also a more effective means to judge the limits of improvements that can be achieved in some situations. This approach has been used effectively in the design of highly loaded airfoils. However, its use in axisymmetric body design has been very limited until recently due to the lack of an adequate inverse-problem solution and to the lack of information about the characteristics of the velocity distributions around low-drag shapes.

The objective in this paper is to demonstrate the use of the inverse-problem approach in the design of low-drag bodies of revolution suitable for large torpedo and small airship applications. Since the primary function of these bodies is to carry a given payload, the one-third power of the volume $V^{1/3}$ is used as a characteristic dimension. The study is carried out

Received April 2, 1980; revision received Oct. 10, 1980.

*Associate Professor, Mechanical Engineering. Member AIAA.
†Design Engineer. Member AIAA.

for a given volume Reynolds number R_V $(=U_\infty V^{1/3}/\nu)$ of 5×10^7. The input velocity distribution for the inverse-problem program is based on a detailed computational study recently carried out by the authors in which they compared the drag characteristics of a number of low-drag shapes suggested by other investigators. The results of this study gave considerable insight to the effect of velocity distribution on drag and body shape. The delay of transition was used as a key for the reduction of drag. Following the trends indicated by this study, a velocity distribution was suggested for input to the inverse-problem program developed by the authors.

Previous Low-Drag Studies

One of the earliest of these is a 1950 study of Gertler[2] who built 24 models of different shapes. These models were tested at various Reynolds numbers by towing them through water at different speeds. The overall drag was measured but the boundary-layer characteristics were not. The purpose of the Gertler study was submarine design which had a volume Reynolds number of approximately 3×10^8. Since the maximum test volume Reynolds number was about 5×10^6, it was necessary to trip the boundary layer at 5% of the body length to simulate the prototype situation. Gertler's study produced a best shape from the 24 models he studied. However, his best-shape model cannot be construed to be an optimum-shape body since an optimization procedure was not followed. The tests by Gertler have been described by Hess[3] as highly accurate and have represented excellent test cases for computational methods over the years.

Carmichael[4] in 1966 developed a new low-drag body by means of shape manipulation. Through his experiments, Carmichael showed that reducing the fineness ratio (FR) has the effect of reducing the surface area and consequently the drag. Then by proper body shaping in analogy with laminar airfoils, a body of FR = 3.33 was deduced from the NACA 66 airfoil series. This tailboomed body (called the Dolphin) was gravity tested in the Pacific Ocean. Drag reduction of 60% was achieved over the conventional torpedo shape for equal volumes at length Reynolds numbers of $2\text{–}3\times10^7$. The primary reason for such significant drag reduction is the strong flow acceleration on the fore part of the body. This acceleration delays boundary-layer transition to a farther aft point on the body. To verify this, transition length Reynolds numbers of $1.4\text{–}1.8\times10^7$ were deduced by comparing the experimental results to computational results. This transition delay proves to be a very effective technique in viscous drag reduction. Hertel[5] considered the shapes of several fast-swimming animals (tunny, trout, dolphin, and shark) as candidates for a low-drag shape for a given volume for VTOL subsonic aircraft applications ($R_L \sim 10^8$). The study indicated that the substantial pressure drop ceases at $x/L \simeq 0.1$ for the tunny and trout shapes which have elliptic noses. Therefore, the chance of sustaining a laminar boundary layer beyond this point is remote at such high Reynolds numbers. On the other hand, shapes with parabolic noses, such as the dolphin and shark, have a strong favorable pressure gradient for a larger distance. Based on these considerations, Hertel developed a new fuselage shape (called Shark 1) which has a 0.22 thickness ratio, sharp nose, and rounded tail. Because of the strong flow acceleration in the range $0<x/L<0.4$, Hertel's transition predictions showed that the boundary layer remains laminar up to $x/L=0.35$ at $R_L \simeq 10^8$. Such a transition delay and the small fineness ratio resulted in a big reduction in drag for a given volume. Parsons and Goodson[6] developed a computer-oriented optimization procedure together with a drag calculation package for the automatic synthesis of minimum drag shapes for a given R_V. A number of suboptimum shapes were developed at different R_V in the range of 5×10^6 to 5×10^7. Two shapes, F2-49 and F-57, with approximately the same drag at $R_V=5\times10^7$ were developed under the condition of a sustained laminar boundary layer (LBL). The Parsons and Goodson study also showed that the drag coefficient $C_{DV}(=2D/\rho V^{2/3}U_\infty^2)$ was insensitive to body shape provided that separation did not occur and that the LBL was not extended. The best turbulent design, body 1-36 at $R_V=5\times10^6$, had about the same drag coefficient as Gertler's best profile. Myring,[7] assuming a completely turbulent boundary layer (TBL), studied the effect of body shape on the viscous drag by changing one parameter at a time. The lowest drag shape, which has continuously changing area distribution, showed a reduction in the drag coefficient based on surface area C_{DS} of as much as 10% over other shapes at the same R_L and for the same FR. Hess,[3] assuming that the boundary layer is turbulent from the nose, developed a simplified drag integral formula based on Truckenbrodt's method for TBLs. Hess's formula was used to study the drag of widely different profile shapes. Hess indicated that C_{DV} is quite insensitive to hull shape and, consequently, some means other than hull shaping should be used in situations when a considerable run of LBLs is not expected. Hess also tried unsuccessfully to use the inverse-problem method of Bristow[8] to design low-drag shapes. He pointed out the lack of information about the characteristics of the velocity distribution needed to produce low-drag profiles. Using a velocity distribution of constant value over most of the body and Bristow's inverse-problem program produced what Hess called "cavitation shapes." The drag performance of these shapes did not show any advantage over prolate spheroids.

Recently, Zedan and Dalton[9] carried out a computational drag study to compare the characteristics of most of the low-drag shapes discussed earlier at R_V of 5×10^7 and 10^8. The study showed that most all of the profiles have $C_{DV}\simeq0.013$ at $R_V=10^8$ assuming a TBL over most of the body. Transition calculations showed that such an assumption is quite accurate; however, it is conceivable to have a short but not negligible run of LBL by increasing the flow acceleration over the first 20% of the body. At $R_V=5\times10^7$, the Zedan and Dalton study showed that all shapes except the Shark and F-57 have early transition and, therefore, are not promising. This part of the study is briefly reviewed later since the present work is based on it.

The Inverse-Problem Method

The inverse problem in hydrodynamics may be stated as follows: given a prescribed velocity distribution, find the body shape that will produce, when placed in a uniform flow, the closest possible velocity distribution to the prescribed one. While there are two other methods in the literature[8,10] to solve this problem, we chose to use our own method[11-13] due to its simplicity. Bristow's method is iterative; the body geometry is updated in each iteration such that the mean square difference between the prescribed velocity distribution and the velocity distribution calculated by the Douglas-Neumann surface source direct method[14] is minimized. The method appears to be quite accurate but it is mathematically tedious, and requires lengthy computations and a large computer facility. As for James' method, a conformal mapping technique is used to transform the body meridian curve into a simpler geometry. The governing partial differential equation that results in the transformed plane is transformed into a number of ordinary differential equations which are solved analytically using a series solution employing sequences of Fourier, Chebyshev, or Legendre functions. An iterative procedure which starts with an initial guess of the body geometry is used to solve the inverse problem. The method converges faster than Bristow's method, however it is mathematically complicated.

The author's method[11-13] is based on representing the axisymmetric body by a source distribution of variable intensity σ_ξ along its axis. The integral equations representing the flowfield due to the source distribution and a uniform stream of velocity U_∞ are

$$\psi(x,r) = -\frac{1}{4\pi}\int_{x_n}^{x_t} \frac{\sigma_\xi\,(x-\xi)\,d\xi}{\sqrt{(x-\xi)^2+r^2}} + U_\infty r^2/2 \qquad (1)$$

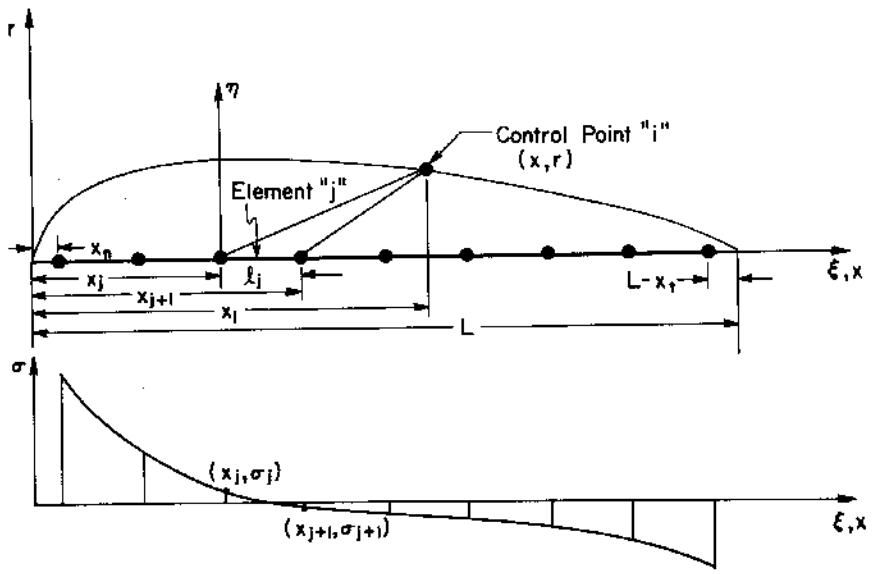

Fig. 1 Definition sketch of elements and singularity distribution for the inverse-problem method.

$$u(x,r) = \frac{1}{4\pi}\int_{x_n}^{x_t} \frac{\sigma_\xi (x-\xi)\,d\xi}{[(x-\xi)^2+r^2]^{3/2}} \tag{2}$$

and

$$v(x,r) = \frac{r}{4\pi}\int_{x_n}^{x_t} \frac{\sigma_\xi\, d\xi}{[(x-\xi)^2+r^2]^{3/2}} \tag{3}$$

where ψ is the stream function at a point (x,r) in the flowfield, and u and v are the axial and radial velocity components at the same points, and x_n and x_t are defined in Fig. 1. Each integral in Eqs. (1-3) can be written as a summation of integrals over N singularity elements distributed between x_n and x_t as shown in Fig. 1. Representing the source intensity over each element by a polynominal of arbitrary degree allows evaluation of the element integrals in closed form. Zedan[15] was able to reduce the integral equations (1-3), when applied at a control point i, to the following algebraic equations:

$$\psi_i = \frac{1}{4\pi}\sum_{j=1}^{M} \bar{\Psi}_{ij} C_j + U_\infty r_i^2/2 \tag{4}$$

$$u_i = \frac{1}{4\pi}\sum_{j=1}^{M} \bar{U}_{ij} C_j + U_\infty \tag{5}$$

and

$$v_i = \frac{r_i}{4\pi}\sum_{j=1}^{M} \bar{V}_{ij} C_j \tag{6}$$

where C_j is a one-dimensional array which includes the polynomial distribution coefficients over all elements, the matrices $\bar{\Psi}_{ij}$, $\bar{U}_{ij}$, and $\bar{V}_{ij}$ are pure functions of profile geometry, and M is the number of the unknown coefficients C_j.

Since the total flow velocity should be everywhere tangent to the body surface, then

$$u_i = \frac{q_i}{\sqrt{1+S_i^2}} \tag{7}$$

where q is the prescribed velocity on the body surface and S is the slope (dr/dx) of the meridian line of the body.

The solution starts with an initial guess of the body geometry; an ellipsoid of high fineness ratio (FR = 16) is satisfactory for most cases. The slope of the meridian line S_i and the matrices $\bar{\Psi}_{ij}$, $\bar{U}_{ij}$, and $\bar{V}_{ij}$ are computed for this geometry. The axial velocity component u_i is then calculated from Eq. (7). The M unknown coefficients C_j are obtained by solving a system of linear equations that consists of the following: 1) Eq. (5) applied at $(M-N)$ control points, 2) $(N-1)$ equations described by the constraint of continuous source intensity at the junction points between the elements, and 3) the closure condition (the net efflux of the source distribution for a closed profile is zero). With the coefficients C_j, the radial velocity distribution v_i is computed from Eq. (6). The new body radius is calculated from Eq. (4) by setting ψ_i equal to zero at all control points; if this fails, a different strategy based on integrating the v_i/u_i array with respect to x is used as described by Zedan.[15] The new profile geometry replaces the initial shape and the calculations are repeated in an iterative manner until convergence is attained. The details of the algorithm and the convergence criteria are given by Zedan. Numerous test cases showed that using a linear intensity variation over all elements except over the last one, where a parabolic distribution is used, gives the best results for most streamlined body shapes.

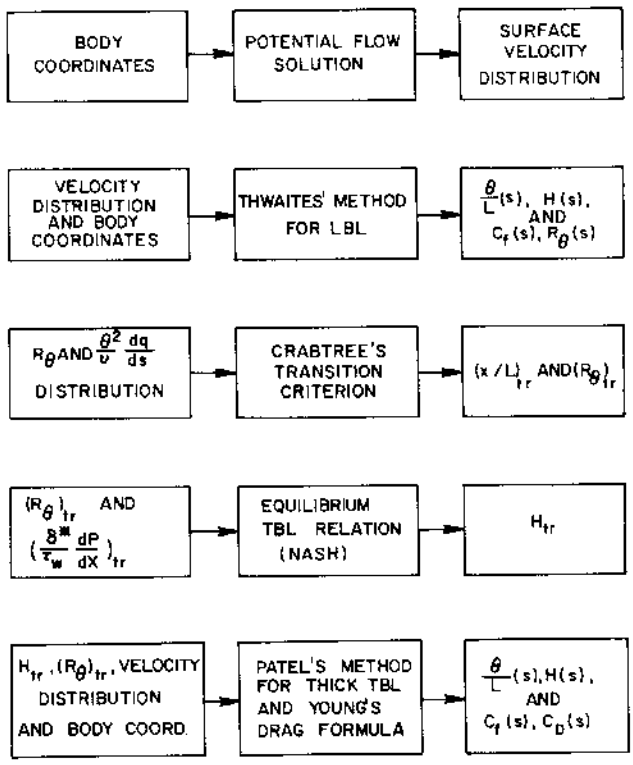

Fig. 2 Block diagram of drag calculation scheme.

Drag Calculation Package

The flow model is standard. At high Reynolds number, the flowfield may be divided into two regions, namely a boundary layer near the body surface and an irrotational region outside the boundary layer. The boundary layer is laminar at the nose and then becomes turbulent at some location downstream. The turbulent boundary layer merges into a wake in the aft body region. The drag is usually computed from the momentum deficit in the wake. The TBL grows much faster than the LBL and is, therefore, responsible for most of the wake momentum deficit and consequently the drag. Using an approximate solution for the flow in the wake, Young[16] related the drag coefficient to the boundary-layer characteristics at the body tail as follows:

$$C_D = \left[\frac{4\pi(r_0\theta)}{A}\left(\frac{q}{U_\infty}\right)^{(H+5)/2}\right]_{TE} \tag{8}$$

where θ is the axisymmetric boundary-layer momentum thickness, r_0 the radius, A a reference area, q the velocity outside the boundary layer, and H the boundary-layer shape factor (ratio of displacement and momentum thicknesses). At the tail of a closed profile, r_0 is zero and θ is infinity although $r_0\theta$ is finite. Thus, Young's formula is applied along the body as $C_D(x)$ to evaluate the limit as the tail is approached. Obviously, the boundary-layer solution and the external velocity distribution are required to compute $C_D(x)$ along the body. A summary of the calculation procedure including the boundary-layer characteristics through the drag computation is shown in Fig. 2.

The external flow velocity distribution $q(x)$ is approximated by the velocity distribution obtained from the potential flow solution around the body. Hess and Smith,[14] Nakayama and Patel,[17] and Smits et al.[18] showed that such an approximation is quite accurate except very close to the tail. The Douglas-Neumann surface source method[14] was initially used to compute the velocity distribution, but now it has been replaced by our refined direct-problem method.[13] Figure 3 shows a good agreement between these two methods for the F-57 and Shark profiles; the only difference is that our method is much simpler and more efficient for axisymmetric bodies. Figure 4 shows further a comparison between the experimental data of Joubert et al.[19] and the velocity distribution obtained by our method.

Thwaites' integral method, as presented by Cebeci and Bradshaw,[20] is used to predict the evolution of the LBL. Comparison with the more exact Cebeci and Smith[21] finite-difference method indicated that the Thwaites' method is quite accurate. Transition is predicted by the Crabtree method[22] which was chosen after a careful consideration of other criteria as discussed by Zedan.[15] Since transition is sensitive to hard-to-control factors, the current predictions may not be physically accurate but we believe the results should be quite good on a comparative basis for different shapes. The TBL calculations are started at the transition location using the value of θ predicted by the LBL solution there and a value for H obtained from the TBL equilibrium relations of Nash.[23,24] The TBL evolution is predicted by Patel's method. This method is quite accurate even for thick boundary layers which is certainly the case near the tail.

The drag package is described in more detail and its results are critically evaluated by Zedan.[15] Comparison with the experimental data of Gertler for profile 4165 of his series 58 showed that the error in the drag coefficient C_{DV} is about 3.2% compared to 9.1% for the predictions of the Parsons-Goodson package in which the LBL and TBL are predicted by the Cebeci-Smith method. The error of the present package was even lower than 3.2% for other test cases (not presented herein), provided the correct transition location is known.

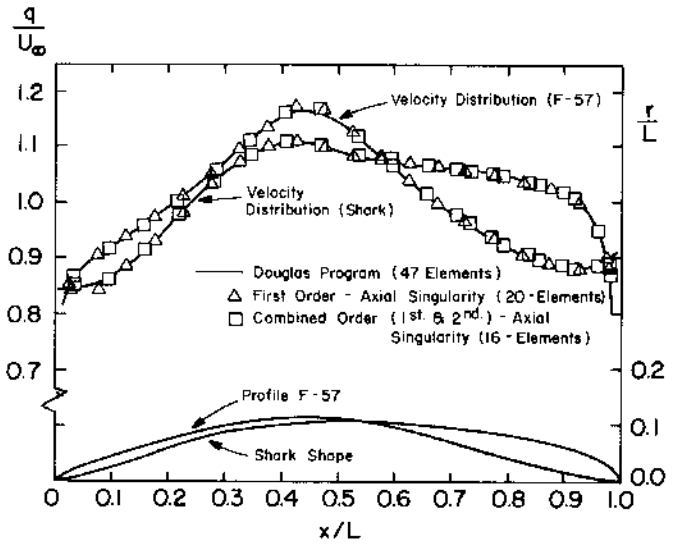

Fig. 3 Potential flow velocity distributions for Shark and F-57 profiles.

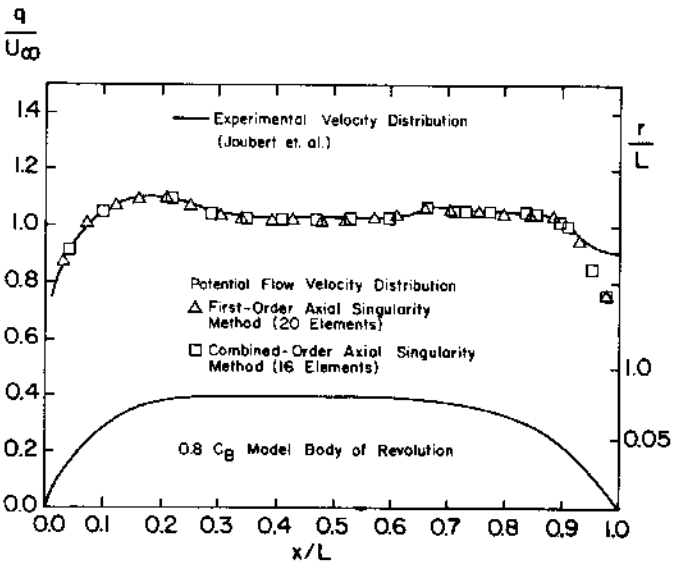

Fig. 4 Experimental and potential flow velocity distribution of $0.8C_B$ tanker body of revolution.

Results and Discussions

Comparing the drag characteristics of a number of the best profile shapes in the literature, our previous study[9] showed that at $R_V = 5\times10^7$ all bodies with the exception of the Shark

Table 1 Summary of results at $R_V = 5\times10^7$

Profile	Tunny	Dolphin	Shark	F-57	F2-49	Myring	I-36	4165
$10^{-8}R_L$	1.8288	2.2646	1.8245	1.8743	1.6096	1.9835	2.3178	2.3529
$(x/L)_{tr}$	0.0987	0.0492	0.3689	0.104 (0.4222)	0.0758	0.0777	0.0965	0.0744
C_{DV}	0.0139	0.0143	0.0114	0.0141 (0.0086)	0.0144	0.0140	0.0135	0.0141

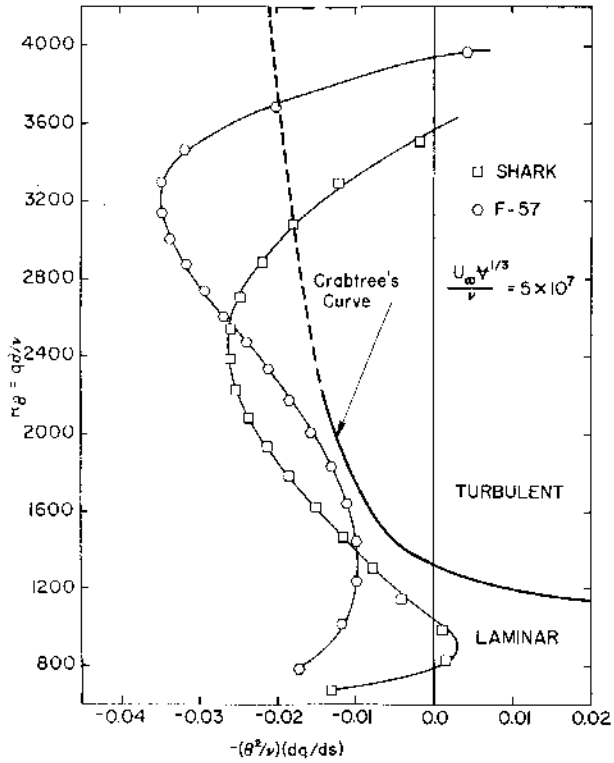

Fig. 5 Transition characteristics of Shark and F-57 profiles, $R_V = 5\times10^7$.

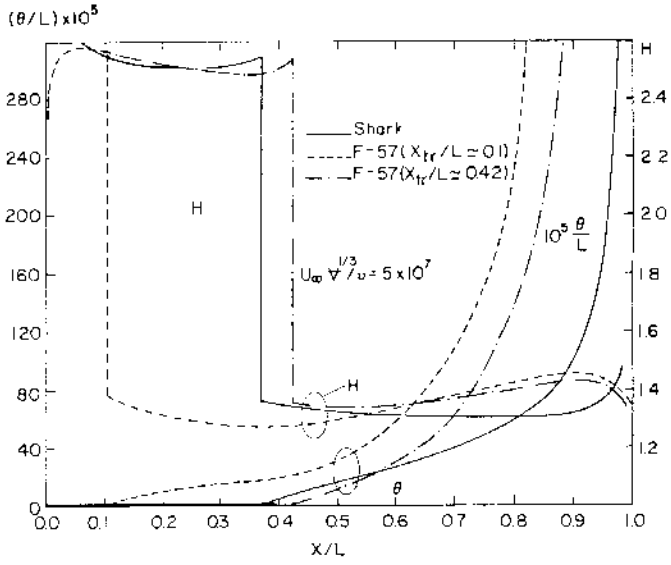

Fig. 6 Boundary-layer development for Shark and F-57 profiles, $R_V = 5\times10^7$.

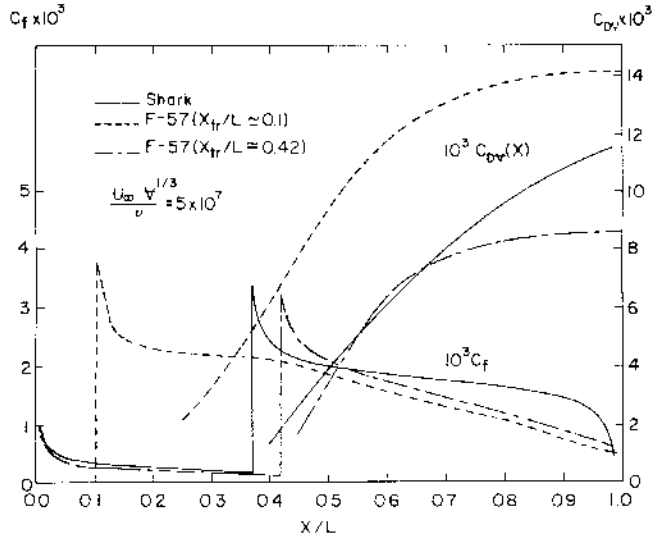

Fig. 7 Variation of friction and drag coefficients along body for cases of Fig. 6.

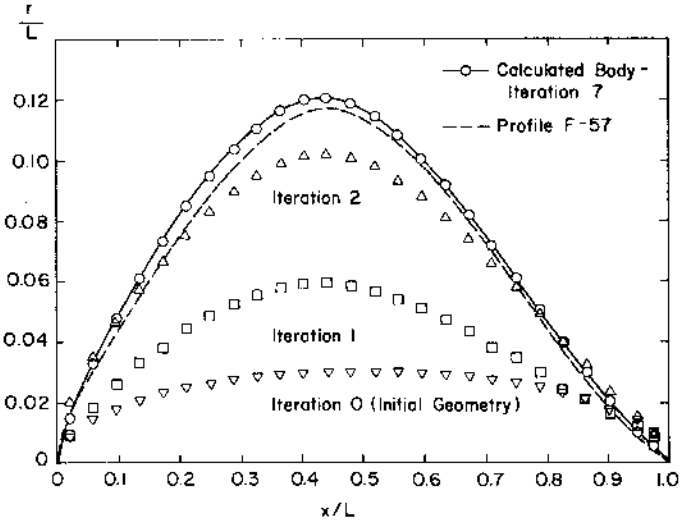

Fig. 8 Inverse problem calculated body shapes at different iterations for modified velocity distribution of Fig. 10.

of Hertel[5] and the F-57 of Parsons and Goodson[6] have transition within the first 10% of the body length and about the same volume drag coefficient ($C_{DV} \simeq 0.014$). Such drag results are summarized in Table 1. The transition location was predicted using the Crabtree criterion. The transition characteristics of the Shark and the F-57 profiles are shown in Fig. 5. No transition is indicated within the limits of the criterion as proposed by Crabtree; however, the curve of profile F-57 comes very close to the Crabtree transition line (in contrast with the Shark shape) in the range $1600 < R_\theta < 2000$. It is conceivable that transition for the F-57 profile may be triggered in that range (which corresponds to $x/L \simeq 0.1$) due to the uncertainty of the Crabtree curve; such uncertainty is a characteristic of all transition criteria. With this early transition for the F-57, the advantage of the Shark shape becomes obvious. However, if such early transition can be avoided, the figure indicates that the transition behavior of the F-57 shape becomes better than for the Shark. In fact, if the Crabtree curve is extrapolated (just for comparison purposes) as shown in the same figure, the transition values of R_θ for the F-57 and the Shark profiles are 3680 ($x/L = 0.42$) and 3080 ($x/L = 0.37$), respectively. The boundary-layer solution for these two shapes is shown in Figs. 6 and 7. Figure 6 shows the evolution of the boundary-layer momentum thickness, θ, and the shape factor, H, while Fig. 7 shows the evolution of the skin friction coefficient C_f ($= \tau_w / \frac{1}{2}\rho q^2$) and $C_{DV}(x)$ along the body surface. The solution for the F-57 profile is shown for the two transition locations mentioned earlier. The predicted value of C_{DV} for the Shark is about 0.0141 while the values for the F-57 profile are 0.0141 and 0.0086 for $x_{tr}/L = 0.1$ and 0.422, respectively.

Based on the above mentioned results, the F-57 shape seems more attractive as a low-drag design for this Reynolds number ($R_V = 5\times10^7$) provided we can insure no transition in the range $0.08 \le x/L \le 0.13$. The inviscid flow velocity distribution for the two shapes shown in Fig. 3 indicates that the velocity gradient, dq/ds, is greater for the Shark in the range $0.07 \le x/L < 0.25$ as compared to the F-57 profile. This provides greater stability for the LBL. So, it appears that a slight modification in the velocity distribution of the F-57 profile, so

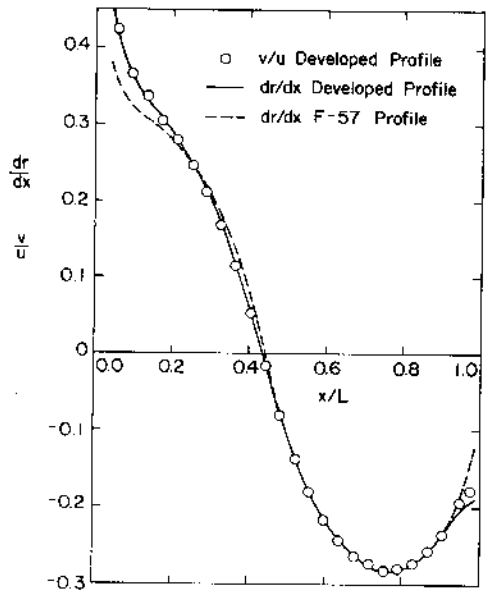

Fig. 9 A comparison of ratio of velocity components v/u calculated in convergence iteration and slope of the meridian line for case of Fig. 8.

Table 2 Coordinates and velocity distribution of the developed profile

x/L	r_0/L	(q/U_∞) [a]	(v/u) [a]	dr_0/dx
0	0	0	–	
0.0192	0.0145	0.7631	0.5334	0.6608
0.0577	0.0327	0.8764	0.4228	0.4305
0.0962	0.0476	0.9207	0.3650	0.3692
0.1346	0.0611	0.9567	0.3357	0.3350
0.1731	0.0734	0.9862	0.3059	0.3070
0.2115	0.0847	1.0191	0.2806	0.2790
0.2500	0.0949	1.0499	0.2469	0.2471
0.2885	0.1037	1.0820	0.2127	0.2107
0.3269	0.1111	1.1145	0.1675	0.1664
0.3654	0.1165	1.1415	0.1152	0.1138
0.4038	0.1198	1.1619	0.0542	0.0531
0.4423	0.1206	1.1671	−0.0137	−0.0134
0.4808	0.1188	1.1538	−0.0800	−0.0784
0.5192	0.1146	1.1267	−0.1366	−0.1345
0.5577	0.1084	1.0953	−0.1809	−0.1795
0.5962	0.1008	1.0634	−0.2165	−0.2150
0.6346	0.0919	1.0319	−0.2432	−0.2421
0.6731	0.0821	1.0021	−0.2631	−0.2615
0.7115	0.0718	0.9747	0.2745	0.2739
0.7500	0.0611	0.9503	−0.2820	−0.2800
0.7885	0.0502	0.9278	−0.2803	−0.2795
0.8269	0.0396	0.9093	−0.2745	−0.2718
0.8654	0.0293	0.8945	−0.2574	−0.2564
0.9038	0.0199	0.8861	−0.2349	−0.2336
0.9487	0.0100	0.8857	0.1943	−0.2002
0.9744	0.0052	0.8921	−0.1780	0.1959
1.0000	0	0	–	

[a] Calculated from the singularity distribution obtained in iteration 7.

as to increase dq/ds in that range, can prevent early transition. The profile which produces the modified velocity distribution can be obtained from the inverse-problem solution.

A New Profile Shape

The modified velocity distribution is shown in Fig. 10. With this velocity distribution as input, the inverse problem method described earlier was used to develop a new profile shape. Twenty-four equal length elements with linear intensity variation and one element of twice the length (of other elements) with parabolic intensity distribution were used. The solution converged quite well. Convergence was almost complete in iteration 4; however the best agreement between

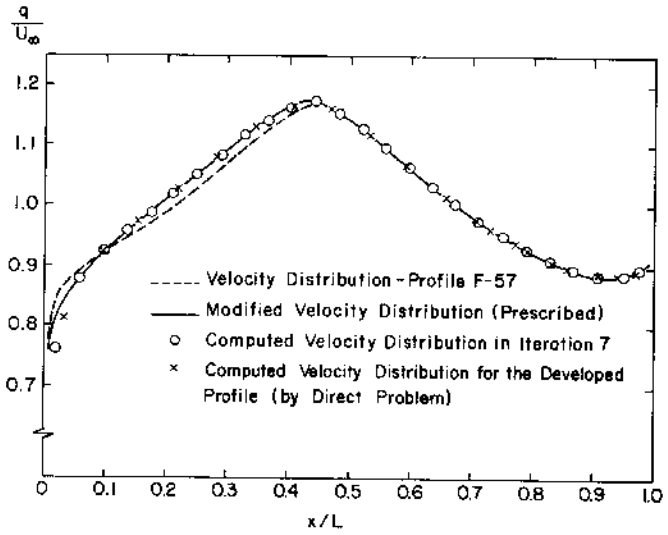

Fig. 10 Prescribed and calculated velocity distributions for developed shape of Fig. 8 and velocity distribution of original F-57 profile.

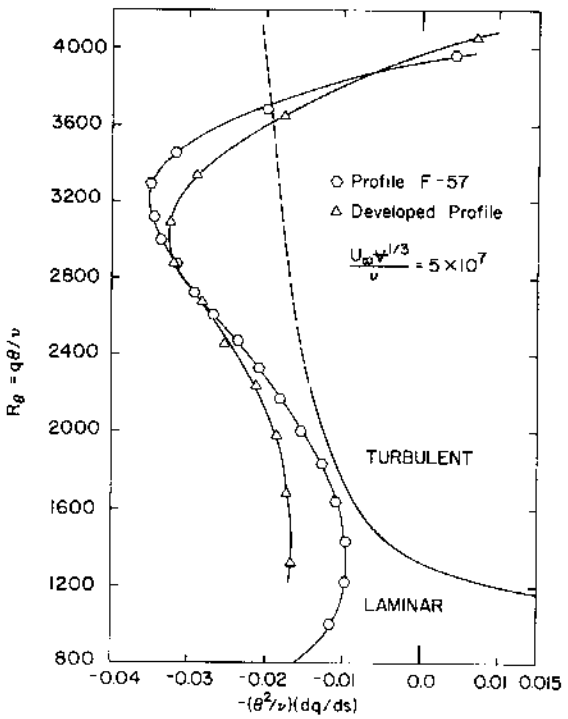

Fig. 11 Transition characteristics of original F-57 profile and developed shape of Fig. 8, $R_\nu = 5 \times 10^7$.

dr_0/dx and v/u occurred in iteration 7. Figure 8 shows the starting geometry (iteration 0) and the calculated body shape at iterations 1, 2, and 7. Also shown in the same figure is the original F-57 profile. Notice that the vertical scale (for r_0/L) is magnified to exaggerate the difference between the new shape (iteration 7) and the F-57 profile. The developed body is thicker than the F-57 profile in the front half, while the two profiles are essentially the same for $x/L > 0.6$. This is expected since the velocity distribution on the rear half has not been altered. Figure 9 and Table 2 show excellent agreement between dr_0/dx and v/u for the developed profile in iteration 7; thus confirming convergence. The variation of dr_0/dx for the F-57 profile is also shown in that figure in order to compare with the new shape. The variation of the slope of the meridian line (dr_0/dx) of the new shape is smoother in the front half as compared to that of the F-57 profile. The calculated velocity distribution in iteration 7 for the new

shape agrees quite well with the prescribed velocity distribution and with the velocity distribution obtained by solving the direct problem (using our method[13]) for the flow around the same body; these are shown in Fig. 10. The coordinates of the new profile as well as the velocity distribution are given in Table 2.

The laminar boundary-layer solution along the surface of the new profile was obtained. Figure 11 shows the transition characteristics of this profile as compared to those of the F-57 profile. While transition is predicted to occur roughly at the same location ($x/L=0.41$) for both profiles, it is very obvious that the new profile has much better capability in resisting early transition. Thus, with the use of the inverse problem, we have achieved our objective of preventing the early transition and therefore kept the drag coefficient at the lower value (0.0086)

Conclusion

The use of the inverse problem in the design of low-drag axisymmetric shapes has been briefly investigated. Comparison of the drag characteristics of a number of the best available profile shapes, at $R_\nu=5\times10^7$, indicated that the Shark shape of Hertel has the lowest drag for a given volume. However, if early transition is avoided, the drag of the F-57 profile becomes even lower than that of the Shark. By modifying the velocity distribution of the F-57 in the front half of the body such that the favorable velocity gradient is increased for $x/L<0.25$, the inverse-problem method of the authors has been used to develop a new profile. The new profile has better transition characteristics than either the Shark or F-57 shapes and consequently a lower drag coefficient.

The modification of the F-57 profile by the inverse method is just an example to demonstrate the potential of developing better shapes by making reasonable modifications in the velocity distributions of some of the available low-drag profiles. However, more information about the properties of the velocity distributions of low-drag shapes is obviously needed in order to make full use of the inverse problem.

References

[1] Huang, C.J. and Dalton, C., "Cargo Transportation by Airships: A Systems Study," NASA CR-2636, 1976.

[2] Gertler, M., "Resistance Experiments on a Systematic Series of Streamlined Bodies of Revolution – For Application to the Design of High-Speed Submarines," David Taylor Naval Ship Research & Development Center, Washington, D.C., Report C-849, 1950.

[3] Hess, J.L., "On the Problem of Shaping an Axisymmetric Body to Obtain Low Drag at Large Reynolds Numbers," *Journal of Ship Research*, Vol. 20, Jan. 1976, p. 51.

[4] Carmichael, B.H., "Underwater Drag Reduction Through Optimal Shape," *Underwater Missile Propulsion*, edited by L. Greiner, Compass Publications, Inc., Arlington, Va., 1966.

[5] Hertel, H., "Full Integration of VTOL Power Plants in the Aircraft Fuselage," *Gas Turbines*, AGARD CP 9, Part 1, 1966.

[6] Parsons, J.S. and Goodson, R.E., "The Optimum Shaping of Axisymmetric Bodies for Minimum Drag in Incompressible Flow," Purdue University Report ACC-72-6, June 1972.

[7] Myring, D.F., "A Theoretical Study of Body Drag in Subcritical Axisymmetric Flow," *Aeronautical Quarterly*, Vol. 28, 1976, p. 186.

[8] Bristow, D.R., "A Solution to the Inverse Problem for Incompressible Axisymmetric Potential Flow," paper presented at AIAA Fluid Dynamics Conference, Palo Alto, Calif., June 1974.

[9] Zedan, M.F. and Dalton, C., "Viscous Drag Computation for Axisymmetric Bodies at High Reynolds Numbers," *Journal of Hydronautics*, Vol. 13, Jan. 1979, p. 52.

[10] James, R.M., "A General Analytic Method for Axisymmetric Incompressible Potential Flow About Bodies of Revolution," *Computer Methods in Applied Mechanics and Engineering*, Vol. 12, 1977, p. 47.

[11] Zedan, M.F. and Dalton, C., "Incompressible Irrotational Axisymmetric Flow about a Body of Revolution: The Inverse Problem," *Journal of Hydronautics*, Vol. 12, Jan. 1978, p. 41.

[12] Zedan, M.F. and Dalton, C., "Potential Flow Around Axisymmetric Bodies: Direct and Inverse Problems," *AIAA Journal*, Vol. 16, March 1978, p. 242.

[13] Zedan, M.F., and Dalton, C., "Higher Order Axial Singularity Distributions for Potential Flow About Bodies of Revolution," *Computer Methods in Applied Mechanics and Engineering*, Vol. 21, 1980, p. 295.

[14] Hess, J.L. and Smith, A.M.O., "Calculation of Potential Flow About Arbitrary Bodies," *Progress in Aeronautical Sciences*, Vol. 8, Pergamon Press, New York, 1967.

[15] Zedan, M.F., "Flow Around Axisymmetric Bodies: The Direct and Inverse Problems," Ph.D. Dissertation, University of Houston, Texas, 1979.

[16] Young, A.D., "The Calculation of Total and Skin Friction Drags of Bodies of Revolution at Zero Incidence," ARC R&M 1874, April 1939.

[17] Nakayama, A. and Patel, V.C., "Calculation of the Viscous Resistance of Bodies of Revolution," *Journal of Hydronautics*, Vol. 8, 1974, p. 154.

[18] Smits, A.J., Law, S.P., and Joubert, P.N., "A Comparison of Theoretical and Experimental Pressure Distributions on Bodies of Revolution," *Journal of Ship Research*, Vol. 24, March 1980, pp. 60-65.

[19] Joubert, P.N., Sinclair, T.J., and Hoffman, P.H., "A Further Study of Bodies of Revolution," *Journal of Ship Research*, Vol. 22, March 1978, p. 54.

[20] Cebeci, T. and Bradshaw, P., *Momentum Transfer in Boundary Layers*, McGraw-Hill Book Co., New York, 1977.

[21] Cebeci, T. and Smith, A.M.O., *Analysis of Turbulent Boundary Layers*, Academic Press, New York, 1974.

[22] Crabtree, L.F., "Prediction of Transition in the Boundary Layer on an Aerofoil," *Journal of Royal Aeronautical Society*, Vol. 62, 1958, p. 525.

[23] Nash, J.F., "Turbulent Boundary Layer Behavior and the Auxiliary Equation," ARC, London, CP 835, 1965.

[24] Nash, J.F., "A Note on Skin-Friction Laws for the Incompressible Turbulent Boundary Layer," NPL Aeronautical Report 1135, 1964.